Journal of Zhejiang University-SCIENCE A (Applied Physics & Engineering)
ISSN 1673-565X (Print); ISSN 1862-1775 (Online)
www.jzus.zju.edu.cn; www.springerlink.com
E-mail: jzus@zju.edu.cn

Group effect in piles under eccentric lateral loading in sand*

Ling-gang KONG[1], Ji-ying FAN[†‡1,2], Jing-wen LIU[1,3], Yun-min CHEN[1]

[1]*Institute of Geotechnical Engineering, College of Architectural and Civil Engineering, Zhejiang University, Hangzhou 310058, China*

[2]*Geoengineering Centre at Queen's-RMC, Queen's University, Kingston, ON, K7L 3N6, Canada*

[3]*Bureau of Housing and Urban-Rural Development of Chengdu, Chengdu 610094, China*

[†]E-mail: jiying.fan@queensu.ca

Received Oct. 31, 2018; Revision accepted Feb. 18, 2019; Crosschecked Feb. 19, 2019

Abstract: Group effect in a pile group under eccentric lateral loading is much more complicated than that in a pile group under lateral loading because the grouped piles have different motion directions due to the twist of the pile cap. The purpose of this study is to develop new *p*-multipliers quantifying group effect in pile groups subjected to eccentric lateral loading. Motions of two individual piles in a pile group under eccentric lateral loading were first studied and concepts of the leading pile and the trailing pile were defined to characterize the relative positions of the two piles. Then centrifuge model tests, numerical analysis, and theoretical analysis were carried out to study the interactions between two piles. It is found that the angles between the motion directions of the leading and trailing piles and the line through both piles, denoted as η and θ, vary in the ranges of 0°–90° and −90°–90°, respectively. The reduction factors of the leading and the trailing piles are both nonlinearly changed with η and θ. The reduction factor of the leading pile is larger than that of the trailing pile if interaction exists. There exist regions on the η-θ plane where the interaction between the two piles is negligible. A concept of critical angle θ_0 was introduced to define the boundary with and without interaction for a given η. Finally, empirical equations of reduction factors and a procedure to calculate *p*-multiplier were proposed and examined using existing test results.

Key words: Pile foundations; Pile groups; Lateral loads; Eccentric lateral loading; Pile-soil-pile interaction; Pile tests
https://doi.org/10.1631/jzus.A1800617 **CLC number:** TU413

1 Introduction

Responses of pile groups subjected to torsional loading and eccentric lateral loading have been investigated in recent years (Kong and Zhang, 2007a, 2008; Gu, 2014; Kong et al., 2015; Chen et al., 2016). Kong and Zhang (2007a, 2008) performed centrifuge model tests on pile groups subjected to torsion. Chen et al. (2016) proposed an analytical method to study the torsional behavior of free-standing pile groups with a rigid pile cap. Gu (2014) conducted centrifuge model tests on pile groups subjected to eccentric lateral loading. Kong et al. (2015) performed 1-*g* (acceleration of gravity) large-scale model tests on a 3×3 pile group subjected to lateral loading with eccentricities of 6*D* and 11*D*, where *D* is the pile diameter. It is found that piles in a pile group subjected to torsional loading or eccentric lateral loading have different motion directions and magnitudes due to the twist of the pile cap, which is much different from a pile group under lateral loading. The piles in a laterally loaded pile group move with the same displacement in the same direction. Therefore, group effect in pile groups subjected to torsion or eccentric lateral loading is imaginably much more complicated than that in pile groups subjected to lateral loading. Nowadays, there is little, if any, study of group effect in pile groups under eccentric lateral loading.

Group effect in pile groups subjected to lateral loading has been studied extensively (Brown et al.,

‡ Corresponding author

* Project supported by the National Natural Science Foundation of China (Nos. 50809060 and 51579218)

ORCID: Ji-ying FAN, https://orcid.org/0000-0002-4632-1980

1988; McVay et al., 1998; Rollins et al., 2005; Reese et al., 2006; Ashour and Ardalan, 2011). Because of the group effect, piles in laterally loaded pile groups undergo larger displacements for a given load per pile than a single isolated pile does. The mechanism of the group effect involves the overlapping of the failure zones formed in front of the individual piles caused by their horizontal motions. One of the most commonly used approaches to characterize the group effect is the *p*-multiplier approach (Brown et al., 1988). In this approach, a constant factor is used to reduce p to obtain p-y curves for piles in a group, where p represents the lateral soil resistance per unit length of the pile and y is the lateral deflection of the pile. This concept is concise and has been incorporated into many numerical codes, such as GROUP (Reese et al., 2006). In practice, *p*-multipliers can be used as a function of pile-row spacing in the loading direction for regular group configurations (McVay et al., 1998). Alternatively, Reese et al. (2006) proposed an equation to calculate the *p*-multiplier of a pile i in a pile group with n piles for arbitrary configurations:

$$f_{mi} = \beta_{1i}\beta_{2i}\cdots\beta_{ji}\cdots\beta_{ni}, \quad j \neq i, \tag{1}$$

where β_{ji} is the reduction factor of pile i due to the adjacent pile j. The reduction factor is defined as the ratio of the pile head horizontal resistance of one pile in a pile group with that of a single pile under the same displacement condition. However, *p*-multipliers for laterally loaded pile groups are hardly suitable for those under torsion or eccentric lateral loading (Kong and Zhang, 2007a; Kong et al., 2015).

The purpose of this study is to develop new *p*-multipliers for group effect in pile groups subjected to eccentric lateral loading. The newly developed *p*-multipliers are called generalized *p*-multipliers in order to differentiate from those for pile groups under lateral loading. In this paper, to study pile-soil-pile interaction due to horizontal motions of two individual piles in a pile group subjected to eccentric lateral loading, the motion feature of two-pile groups subjected to eccentric lateral loading is analyzed in detail. Then, centrifuge model tests, numerical analysis, and a newly developed soil failure model on pile-soil-pile interaction between two piles are introduced. Finally, empirical equations for reduction factors and a procedure are proposed to calculate *p*-multiplier of each pile in a pile group under eccentric lateral loading. Data from reported model pile group tests are used to verify the accuracy of the proposed approach.

2 Motions of piles in pile groups under eccentric lateral loading

2.1 Pile cap motion

For a pile group under eccentric lateral loading, if its cap is stiff enough to be considered as rigid and the overturning angles of the pile cap in two horizontal directions are negligible, the motion of the pile cap is considered as a plane motion of a rigid body. Thus, there exists a twist center in the motion plane of the cap at any time, called the instantaneous center, and the direction of the instantaneous velocity of a point in the cap is perpendicular to the connection line between the point and the instantaneous center.

Fig. 1 illustrates the motion of a pile in a pile group subjected to a lateral load with an eccentricity. Assume that the instantaneous center of the pile group is unchanged under the given loading. The pile rotates from the initial position through an angle δ to the final position. The pile displacement is $\boldsymbol{s}$ and the instantaneous velocity of the pile at the initial position is $\boldsymbol{v}$. The angle between $\boldsymbol{s}$ and $\boldsymbol{v}$ is half of the rotation angle δ. If δ is small, the direction of $\boldsymbol{s}$ can be approximated to that of $\boldsymbol{v}$. In fact, the tests conducted by Kong et al. (2015) and Gu (2014) show that the locus of the pile head approximately kept straight throughout the whole loading process, which implies that the direction of the instantaneous velocity of each pile in the pile group was almost consistent with that of the pile-head displacement for twist angles up to 12°. Therefore, for a pile group twisted several degrees, the displacement direction of a pile in the pile group can be approximately figured out according to the position of the instantaneous center of the pile group.

2.2 Motions of two piles

Since both pile group configuration and applied forces transferred to pile groups by eccentric lateral loading are arbitrary, the instantaneous centers of the pile groups could be anywhere in the plane of the pile caps. Provided that a two-pile group subjected to

eccentric lateral loading rotates clockwise about an instantaneous center, as shown in Fig. 2, the plane that the instantaneous center locates, is divided into six sections by aa′, bb′, and cc′. An arrow at a pile center in Fig. 2 represents the vector of instantaneous velocity of the pile. As the instantaneous center is in the sections between bb′ and cc′ (e.g. points A and B), the two piles move to different sides of aa′ (Fig. 2); while the two piles move to the same side of aa′ if the instantaneous center is in the left side of bb′ or the right side of cc′ (e.g. points A' and B'). As the instantaneous center is located at bb′ or cc′, one of the two piles moves parallel to aa′ or has no motion, while another

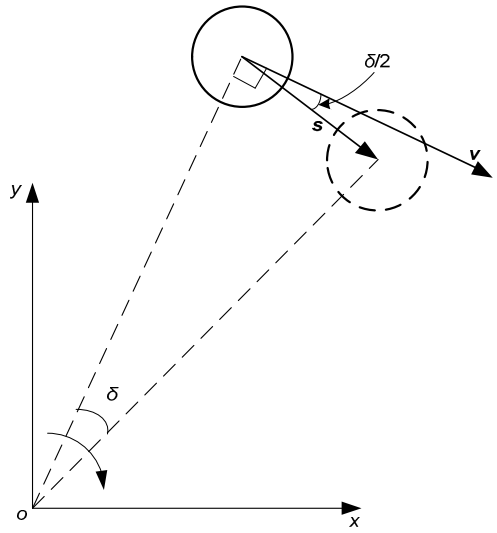

Fig. 1 Motion of a pile rotating around an instantaneous center

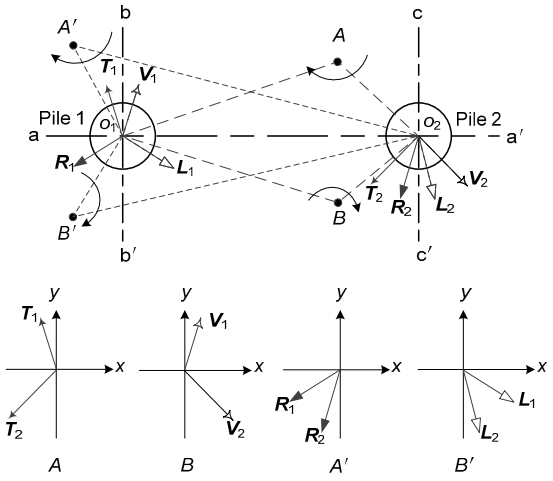

Fig. 2 Motion directions of two piles

can move to either side of aa′ according to the position of the instantaneous center. When drawing both vectors in a x-y coordinate system, where the x axis is parallel to aa′, as shown in Fig. 2, the two vectors are either in the same quadrant or distribute in the two adjacent quadrants symmetric about the x axis. A feature is that both the component vectors of the instantaneous velocities along aa′ are in the same direction if both are non-zero. If the rotation direction of the two-pile group is assumed anticlockwise, the same feature can be obtained through a similar analysis.

To describe the motions of the two piles shown in Fig. 2 in a convenient way, the two piles are defined as a leading pile and a trailing pile. Taking the directions of both component vectors along the connection line between the two piles as a reference, if one of the two components along the connection line is a non-zero vector and points to a pile, the pile pointed to is called the leading pile while the other pile is the trailing pile. Conversely, if a pile is located at the opposite direction of the non-zero component vector, the pile is the trailing pile, and the other is the leading pile. If the components of both instantaneous velocities along the connection line are zero vectors, the two piles can be designated arbitrarily. Taking the two piles in Fig. 2 as an example, Pile 1 is the leading pile and Pile 2 is the trailing pile as their instantaneous center is above aa′; conversely, Pile 1 becomes the trailing pile and Pile 2 is the leading pile as the center is below aa′. Therefore, a pile in a pile group could be both the leading pile relative to an adjacent pile and the trailing pile relative to another.

Suppose η is the angle between the motion direction of the leading pile and the line connecting the leading pile and the trailing pile, as shown in Fig. 3. Regardless of its rotation direction, η is designated as positive and varies in the range of 0°–90°. Define θ as the angle between the motion direction of the trailing pile and the connection line (Fig. 3). Referring to Fig. 2, if the vectors of the leading pile and the trailing pile are at the same side of the connection line, θ is defined as positive; while θ is negative if they are at different sides, so the value of θ varies between −90° and 90°. Any condition of motion directions of two piles in a pile group subjected to eccentric lateral loading can be represented by a combination of η and θ.

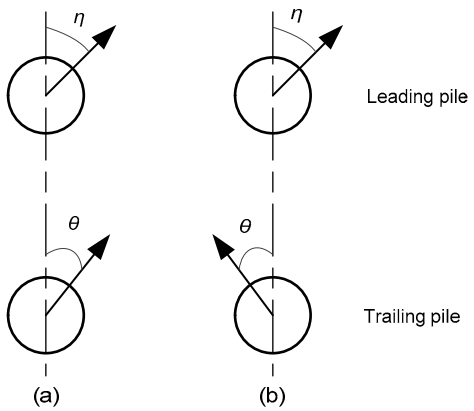

Fig. 3 Relationship between η and θ
(a) $\theta \geq 0$; (b) $\theta < 0$

3 Centrifuge model tests

3.1 Test equipment

Centrifuge model tests were performed to investigate pile-soil-pile interactions between two piles simultaneously subjected to lateral loads in different directions in the ZJU-400 geotechnical centrifuge. A test system was developed which included two lateral loading devices and displacement measurement devices. The system was arranged in a large rigid model container with inside dimensions of 1.2 m×0.95 m×1.0 m, as shown in Fig. 4.

A lateral loading device included an electric motor, a reduction gear box, a direction controller, an Entran-type load cell, an extension bar, and a loading ring. The direction controller connected the electric motor and the gear box. The motion direction of the output shaft of the gear box was adjustable by means of the direction controller to enable horizontally loading a model pile in a desired direction. The direction controller was fixed at the bottom of a double-beam fixing frame, which transferred the horizontal reaction forces to the container (Fig. 4a). A load cell was used to measure the load applied on the model pile head, and an aluminum bar was used to connect the output shaft and the load cell. The length of the bar was adjustable so that the loading device could be used in different loading cases. As shown in Fig. 4b, a loading ring with an internal diameter of 15 mm was fixed in front of the load cell, and was capable of horizontally pushing or pulling a model pile based on the test requirements. To mount the loading ring on a model pile, the model pile was first passed through the loading ring, then the extension bar was adjusted to have the inner side of the loading ring just touch the outside surface of the model pile. Two lateral loading devices were needed in a two-pile test. A laser sensor was used to measure the pile head horizontal displacement of each model pile. As shown in Fig. 4b, an aluminum plane fixed on each loading ring was utilized as the laser reflective surface; the data measured from the laser sensor represented the lateral displacement of the pile.

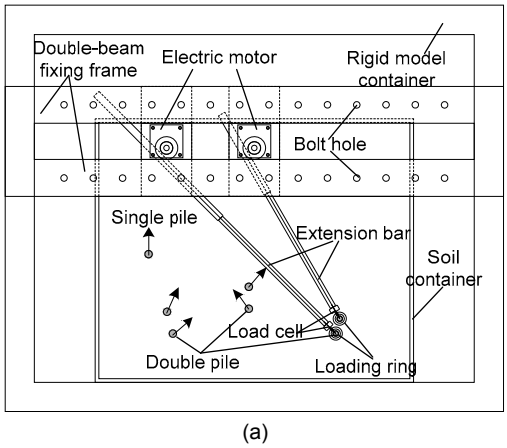

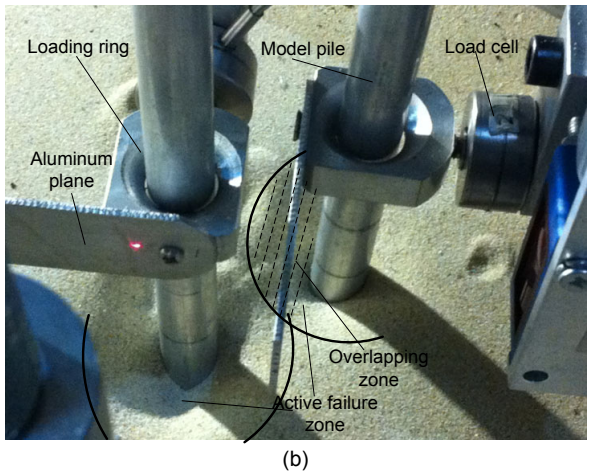

Fig. 4 Layout of the test system
(a) Configuration of TG-3; (b) Overlapping of the failure zones (η=45° and θ=−45°)

3.2 Model piles and model sand

Seven model piles were made using aluminum tubes 850 mm in length, 14 mm in outside diameter, and 1.5 mm in wall thickness. The pile toes were

circular truncated cones 2 mm in bottom diameter and 7 mm in length. The embedded length was 700 mm. The model piles were tested at 40*g* to simulate prototype concrete piles with dimensions 0.56 by 28 m in diameter and embedded length and flexural stiffness of 203 MN·m^2. Since the purpose of these model tests was to investigate pile-soil-pile interactions between two piles, the plastic response of the modeled concrete piles was ignored in the simulation; this is the usual treatment in centrifugal modeling. This treatment is necessary in model testing to study the pile-soil-pile mechanism only. Concrete model piles will be considered in studying the failure mechanism of foundations (Hu et al., 2006; Cai, 2011).

The sand examined can be classified as poorly graded sand according to the unified soil classification system, with a specific gravity of 2.633. The particle-size diameters corresponding to 10%, 30%, and 60% passing on the cumulative particle-size distribution curve are 0.11, 0.14, and 0.19 mm, respectively. The critical friction angle measured by the sand pile test is 32°. A single-hose raining method was used to prepare the samples with a depth of 750 mm (Kong and Zhang, 2007b). A soil container with inner dimensions of 850 mm×700 mm×750 mm in length, width, and depth, respectively, was made of steel plates with a thickness of 10 mm. Sand beds of two relative densities were prepared for the tests. Table 1 summarizes the key parameters of the soil.

3.3 Test procedure and test plan

Six loading cases, as shown in Fig. 5, were selected for the present study. The spacing of the two piles in the six cases is three times the pile diameter (3*D*). The six loading cases were equally divided into two loading series by two values of η, 0° and 45°, respectively. Eight two-pile tests were conducted successfully. Table 1 summarizes the eight tests in three test groups, denoted as TG-1, TG-2, and TG-3, based on the loading series and soil densities. TG-1 and TG-2 were conducted in sand with a relative density of 60%, while TG-3 was in sand with a relative density of 45%. The two loading cases in TG-2 were the same as the corresponding cases in TG-3 as a comparison to study the effect of soil density on pile-soil-pile interaction.

Fig. 4a shows the test configuration of TG-3 (corresponding to the loading series with η=45°). Three two-pile groups and a single pile were tested in TG-3. The solid points in Fig. 4a represent the positions of the model piles and the arrows indicate the loading directions. To avoid boundary effects and soil disturbance, the distances between any two test spots and between the test spots and the container boundaries were at least 10 times the pile diameter (Craig and Sabagh, 1994). Before accelerating the centrifuge, the seven model piles were vertically jacked at a velocity of 2 mm/s into the soil to 700 mm at their designed positions using a pile-jacking device. After assembling the test system for a loading case, the centrifuge was accelerated to 40*g*. After the settlement of the soil bed had been completed, both model piles were simultaneously loaded at a speed of 0.1 mm/min. The loading point was 50 mm above the ground. After completing one loading case, the centrifuge was stopped and the test system was disassembled and reassembled for the next one.

4 Numerical simulation

ABAQUS was employed to further investigate the influence of η and θ on pile-soil-pile interactions between two piles. Both the pile shafts and the soil domain in the numerical model were represented by 3D solid elements with 8-node linear brick, and a

Table 1 Summary of centrifuge tests and soil parameters in the numerical model

Test group	Loading condition		Soil parameter			
	η (°)	θ (°)	Relative density (%)	Peak friction angle (°) (Bolton, 1986)	Young's modulus at pile tip (MPa)	Poisson's ratio
TG-1	0	0, 45, 90	60	35.7	16.0	0.22
TG-2	45	30, 60	60	35.7	18.0	0.22
TG-3	45	30, 60, −45	45	34.2	13.2	0.22

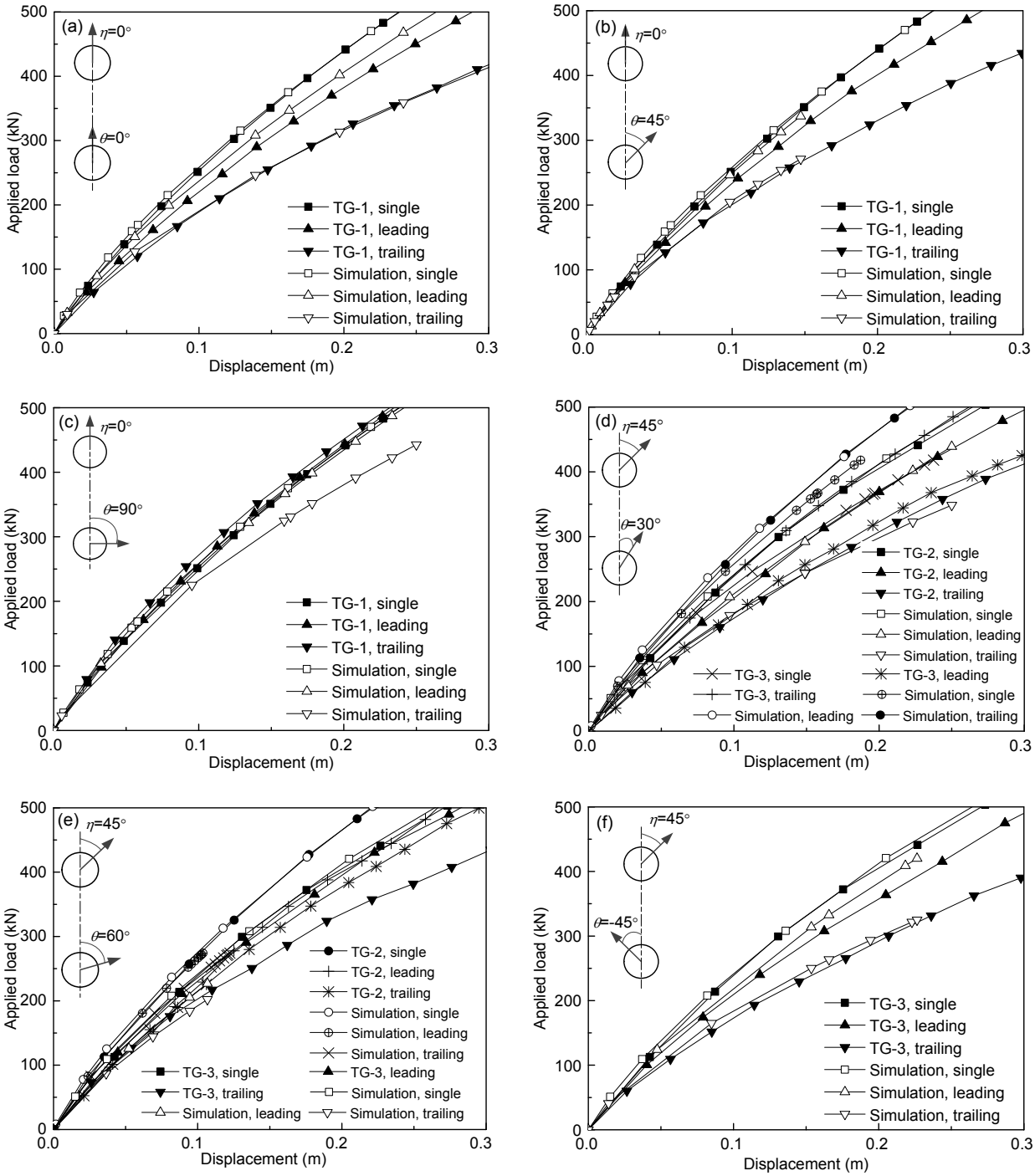

Fig. 5 Applied load-displacement curves

(a) Case 1 (η=0° and θ=0°); (b) Case 2 (η=0° and θ=45°); (c) Case 3 (η=0° and θ=90°); (d) Case 4 (η=45° and θ=30°); (e) Case 5 (η=45° and θ=60°); (f) Case 6 (η=45° and θ=−45°)

mesh refinement was performed in the positions where high levels of strain were expected to occur. A single-pile model and a double-pile model were built to simulate the prototype piles in the present tests. The pile shafts were assumed to be elastic with a Young's modulus of 42 GPa and a Poisson's ratio of 0.33. The soil was modeled with a Mohr–Coulomb constitutive model. The peak friction angle of the model sand was

taken as the soil friction angle in the model, which was calculated by the following empirical correlation proposed by Bolton (1986):

$$\varphi_{\max} = \varphi_{\text{crit}} + 3D_{\text{r}}\left[(10 - \ln p) - 1\right], \tag{2}$$

where φ_{crit} is the critical friction angle, D_{r} is the relative density of sand, and p is the effective mean normal stress at failure. It is assumed that Young's moduli of the soil linearly increase with depth. Young's moduli of soil were back-analyzed from the results of the single pile tests in each test group. Table 1 summarizes the employed soil parameters. Because of the slight difference of the responses of the single piles in TG-1 and TG-2, the back-calculated Young's moduli of soil for TG-1 and TG-2 were also different. Two different sets of nodes were defined at the pile-soil interface to enable the modeling of the frictional contact for Mohr–Coulomb model. A friction coefficient of 0.493 was used in the sliding contact model. Separation between pile and soil took place once a tensile force developed at the interface. To eliminate the boundary effect, the total depth of soil mesh was 40 m and the lateral edges of the domain were 32 m. A displacement-controlled loading mode was adopted in the numerical analysis.

Besides the six loading cases in Table 1, another ten loading conditions, θ=0° and 90° in the case of η=45°, and θ=−75°, −30°, −15°, 0°, 15°, 30°, 60°, and 90° in the case of η=90°, were simulated by the developed numerical model. Soil parameters in the case of η=90° were in accordance with those in TG-1.

5 Experimental and numerical results

Fig. 5 shows the load-displacement curves obtained from the model tests. It is found that the resistances of the leading and trailing piles are lower than that of the single pile in all loading cases except Case 3 (η=0° and θ=90°), which demonstrates that there exist significant pile-soil-pile interactions in all the cases except Case 3. In Case 3, the curves of the leading and trailing piles almost coincide with that of the single pile (Fig. 5c). In addition, the lateral resistance of the trailing pile is smaller than that of the corresponding leading pile in all the cases except Case 3, which implies that the pile position also affects the pile-soil-pile interactions. Numerical results are also shown in Fig. 5 for comparison. Most of the numerical curves match the corresponding test data well. The most significant difference between both results is observed in Case 3. The numerical curve of the leading pile matches the test curve well, but that of the trailing pile is lower than the test curve. It demonstrates that the numerical model slightly overestimated the soil response in front of the trailing pile, especially in the cases where small or no pile-soil-pile interaction exists between the two piles.

Fig. 6 shows the reduction factors β obtained from the experimental and numerical curves in Fig. 5. Let β_{l} and β_{t} represent the reduction factors of the leading and trailing piles, respectively. All β were calculated at the pile head displacement of 150 mm (0.27D), where β became constant, except the numerical results in the case of η=45° and θ=60°. In this case, β_{l} and β_{t} were calculated at a pile head displacement of 100 mm since a pile head displacement of 150 mm was not obtained from the numerical analysis. The experimental β on in-line (η=θ=0°) and side-by-side (η=θ=90°) pile groups with pile spacing 3D in sand reported by Reese et al. (2006) and Fayyazi et al. (2012), as well as the predicted β at η=θ by the empirical equations proposed by Reese et al. (2006), are also shown in Fig. 6. The data are generally in agreement with the present experimental and numerical results. Both β_{l} and β_{t} in all the cases change nonlinearly with θ. In addition, as shown in Figs. 6b and 6c, both β_{l} and β_{t} in the cases of η=45° and 90° are asymmetric with respect to the y-axis.

Comparing TG-2 in sand with a relative density of 60% and TG-3 in sand with a relative density of 45%, both β_{l} and β_{t} in the case of θ=30° are 0.88, 0.69 and 0.88, 0.74, respectively, and those in the case of θ=60° are 0.86, 0.81 and 0.96, 0.81, respectively. Those from the numerical results are equal, and are 0.89 and 0.74 in the case of θ=30° and 0.92 and 0.80 in the case of θ=60°. It seems that the soil density has little influence on the reduction factors in the investigated range of soil relative density. Because of the complexity of interaction between two piles, the effect of soil density needs further study.

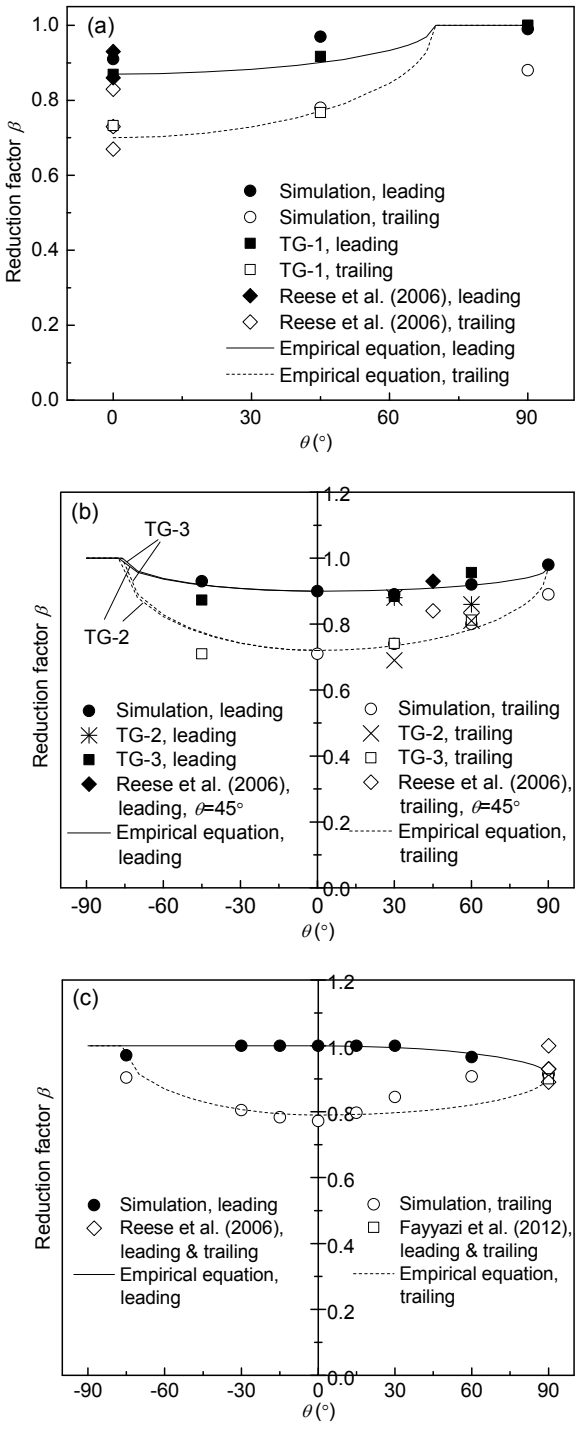

Fig. 6 β-θ curves
(a) η=0°; (b) η=45°; (c) η=90°

Fig. 4b shows a photograph of soil surface collapse around two model piles. The failure zone at the opposite side of the loading direction behind each model pile formed an arch contour. The failure zone, caused by stress relaxation generating active earth pressure along the pile shaft (Reese et al., 1974; Otani et al., 2006), is called the active failure zone. The radius of the failure zones was approximately 1.5D in both soil relative densities. Otani et al. (2006) employed X-ray computed tomography (CT) to investigate the failure pattern of a laterally loaded single pile in dry sand. Two failure zones around the pile were observed. One is the active failure zone, and the other is a failure zone in front of the pile, called the passive failure zone by Reese et al. (1974). The sizes of both the failure zones decreased with depth, and the depths of both are approximately equal. It is also found from Fig. 4b that there is an overlapping zone between the passive failure zone in front of the trailing pile and the active failure zone behind the leading pile. As mentioned before, "overlapping" is the mechanism of the group effect in laterally loaded pile groups caused by their horizontal motions. In pile groups under torsional loading or eccentric lateral loading, the "overlapping" phenomenon is complicated because of the different motion directions and magnitudes of the piles in the groups. For two piles in a pile group under eccentric lateral loading, like Fig. 3, the overlapping zone between both piles is relevant to their motion directions, denoted by η and θ, respectively, so the pile-soil-pile interaction of the two piles changes with η and θ.

6 Critical angles for pile-soil-pile interaction between two piles

Taking η and θ as two axes, a rectangular coordinate system is formed by η and θ, called the η-θ plane. The test data from Case 3 indicate that at least a region exists on the η-θ plane, where no pile-soil-pile interaction between two piles exists, so a soil failure model was developed to find the boundary between the regions with and without interaction. A passive wedge-type failure model proposed by Brown et al. (1988) is employed to illustrate the failure zones in front of both piles, as shown in Fig. 7a. For convenience and a conservative view, the spreading angle of the wedge is taken as the internal friction angle φ although it is probably related to soil density (Reese et al., 1974). The active failure zones behind both piles are assumed to be "U" shape with a radius R (Fig. 7a).

It is assumed that the passive zone of the trailing pile overlaps with both of the failure zones of the leading pile but the active zone of the trailing pile never overlaps with both. Employing the developed soil failure model to analyze the overlapping of the failure zones between two piles, three possible critical conditions were determined (Fig. 7).

In the region of $90°\geq\eta\geq0°$ and $90°\geq\theta\geq0°$ (the upper half of the η-θ plane), as shown in Fig. 7a, for a given value of η, the critical condition is that the left side of the wedge failure zone of the trailing pile is parallel to the right side of the wedge failure zone of the leading pile. The corresponding value of θ is called the critical angle and denoted as θ_0. Referring to Fig. 7a, $\theta_0=\eta+2\varphi$. As θ is lesser than θ_0, an overlapping zone between the leading and trailing piles is generated. It should be noted that θ_0 should be smaller than 90°, so there is no interaction in the range of $90°\geq\theta\geq\theta_0$. Take two-pile groups with pile spacings of $3D$ and $5D$, respectively, as examples. Fig. 8 shows variations of θ_0 on the η-θ plane as φ are 32° and 35°, respectively. Regardless of pile spacing, the region without interaction only exists at the top left corner of the η-θ plane. The region without interaction disappears when φ is larger than 45°.

Figs. 7b and 7c show two critical conditions in the range of $90°\geq\eta>0°$ and $0°>\theta\geq-90°$ (the lower half of the η-θ plane). As $\eta\geq\varphi-\xi$, where ξ is the angle between the line connecting the two piles and the common tangent between the trailing pile and the active failure zone of the leading pile (Fig. 7b), the critical condition is the position where the right side of the wedge zone of the trailing pile touches the edge of the active failure zone of the leading pile, where the critical angle is $\theta_0=-(\varphi+\xi)$. The region without interaction is in the range of $\theta_0>\theta>-90°$ if $\theta_0>-90°$. If $\varphi-\xi>0°$ and $\varphi-\xi>\eta$, the critical condition is the position where the right side of the soil wedge zone of the trailing pile is parallel to the left side of the wedge zone of the leading pile. Referring to Fig. 7c, the critical angle is $\theta_0=-(2\varphi-\eta)$. If $\theta_0>-90°$, there also exists a region without interaction in the range $\theta_0>\theta\geq-90°$.

Referring to Fig. 7b, ξ can be calculated by

$$\xi=\arcsin\left(\frac{0.5D+R}{L}\right), \tag{3}$$

where L is the pile spacing. If assuming the slip lines of the active failure zone are straight, the angle

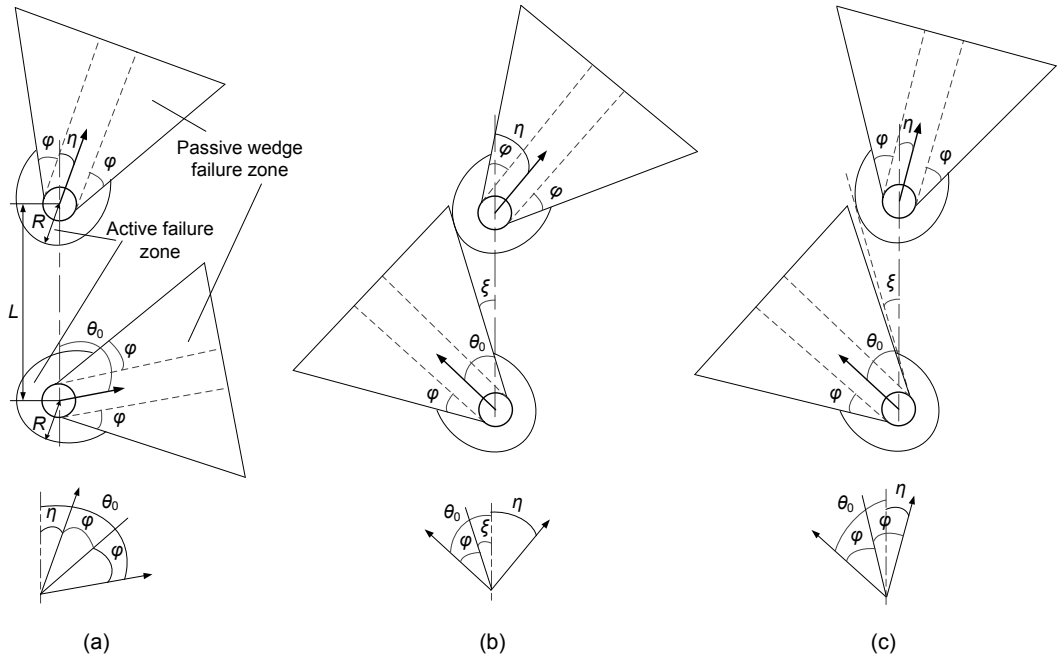

Fig. 7 The critical conditions of two piles with different motion directions
(a) $90°-2\varphi\geq\eta\geq0°$ and $\theta\geq0°$; (b) $\eta\geq\varphi-\xi$ and $\theta<0°$; (c) $\varphi-\xi>\eta$ and $\theta<0°$

between the slip lines and vertical direction is $45°-\varphi/2$ (Cheng and Hu, 2005), so

$$R = H\tan\left(45°-\frac{\varphi}{2}\right)+\frac{D}{2}, \tag{4}$$

where H is the depth of the active failure zone, which, as mentioned before, is approximately equal to the wedge depth of the passive failure zone. Reese et al. (2006) plotted H varying with φ. It is found from Eq. (4) that R is not sensitive to φ. For instance, R increases from $9.2D$ to $10.2D$ as φ increases from 30° to 45°. As pointed out by Reese et al. (2006), the significant difference between the calculated result and the test data may come from the elementary nature of the models used in the computation; even so, the equation serves a useful purpose in indicating the form if not the magnitude. A correction coefficient 0.16 is introduced into the first phase in Eq. (4), which was back-calculated based on the observed radius of the active failure zone in the present tests.

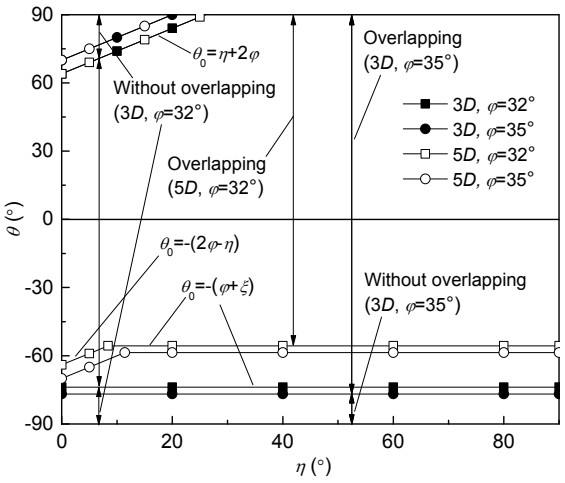

Fig. 8 Variations of θ_0 on the η-θ plane

Fig. 8 also shows variations of θ_0 in the region of $0°>\theta\geq-90°$. As the pile spacing is $3D$, ξ, calculated by Eq. (3), is equal to 41.8°, which is larger than φ (32° and 35°), so $(\varphi-\xi)$ is negative. Since η is positive and always larger than $(\varphi-\xi)$, θ_0 is calculated by $\theta_0=-(\varphi+\xi)$. As the pile spacing is $5D$ (ξ=23.6°), the θ_0-η curves are segmental lines and are calculated by $\theta_0=-(2\varphi-\eta)$ in the range where $\varphi-\xi>\eta>0°$ (Fig. 8).

In the interesting range of φ from 30° to 45°, the radius of the active failure zone R is around $1.5D$. If the pile spacing is less than $3D$, overlapping will occur between the active failure zones caused by the leading and trailing piles. The analysis in Fig. 7 ignores the overlapping between the active failure zones, so the developed approach is suitable for pile groups with pile spacing of approximately $3D$ or larger. In addition, the maximum pile spacing is the distance at which the interaction is ignored as the two piles are in an in-line arrangement. Rollins et al. (2005) and Ashour and Ardalan (2011) summarized the variations of p-multiplier with pile spacing from different researchers and agencies, which indicates that the utmost pile spacing is $8D$. Conservatively, $8D$ is taken as the maximum pile spacing. Table 2 summarizes the equations of θ_0 in different ranges of the η-θ plane as φ is smaller than 45° and L is between $3D$ and $8D$.

7 Calculation of *p*-multiplier

7.1 Empirical equations of the reduction factor

As shown in Fig. 6, both β_l and β_t are asymmetric with the y-axis in general, so they need to be studied separately in the ranges $0°>\theta\geq-90°$ and $90°\geq\theta\geq0°$. The critical angles θ_0 can be calculated based on the equations in Table 2 for a given η. For the investigated loading cases with η=0°, 45°, and 90° in this study, φ

Table 2 b and θ_c in β calculation as $\varphi<45°$ and $8D\geq L\geq 3D$

η-θ plane		θ_0	θ_c	b_l	b_t
$90°\geq\theta\geq0°$	$90°-2\varphi\geq\eta\geq0°$	$\eta+2\varphi$	θ_0	1	1
	$90°\geq\eta>90°-2\varphi$	–	90°	$1-\dfrac{(1-b_{90})(\eta+2\varphi-90°)}{2\varphi}$	b_{90}
$0°>\theta\geq-90°$	$90°\geq\eta\geq\varphi-\xi$	$-(\varphi+\xi)$	θ_0	1	1
	$\varphi-\xi>\eta>0°$	$-(2\varphi-\eta)$	θ_0	1	1

is taken as the peak friction angle listed in Table 1. Through a trial-and-error procedure, β_l and β_t in Fig. 6 were well-fitted by a series of ellipse formulas. Thus, β_l and β_t for a given η are expressed as:

$$\beta_l=\begin{cases} b_l-\dfrac{b_l-a_l}{|\theta_c|}\sqrt{\theta_c^2-\theta^2}, \\ \qquad 0>\theta\geq\theta_c \ \text{ or } \ \theta_c\geq\theta\geq 0, \\ 1, \\ \quad 0>\theta_c\geq\theta\geq -90^\circ \ \text{ or } \ 90^\circ\geq\theta\geq\theta_c>0, \end{cases} \tag{5}$$

$$\beta_t=\begin{cases} b_t-\dfrac{b_t-a_t}{|\theta_c|}\sqrt{\theta_c^2-\theta^2}, \\ \qquad 0>\theta\geq\theta_c \ \text{ or } \ \theta_c\geq\theta\geq 0, \\ 1, \\ \quad 0>\theta_c\geq\theta\geq -90^\circ \ \text{ or } \ 90^\circ\geq\theta\geq\theta_c>0, \end{cases} \tag{6}$$

where a_l and a_t are the values of β_l and β_t at θ=0° for a given η, respectively; b_l and b_t represent the values of β_l and β_t at $\theta=\theta_c$ for a given η, respectively; θ_c is a reference factor. If θ_0 exists on the η-θ plane, $\theta_c=\theta_0$; otherwise, θ_c=90° in the range of 90°≥θ≥0° and θ_c=−90° in the range of 0°>θ≥−90°.

Fig. 9 illustrates the variations of β with η at θ=0° obtained from the model tests, numerical results, and references. Functions of quadratic parabola were employed to best fit the data points of the leading and trailing piles, which are

$$a_l=a_{l0}+(1-a_{l0})\left(\frac{\eta}{90}\right)^2, \tag{7}$$

$$a_t=a_{t0}+\min(0.09,1-a_{t0})\left(\frac{\eta}{90}\right)^2, \tag{8}$$

where a_{l0} and a_{t0} are two constants. The physical meanings of a_{l0} and a_{t0} are the reduction factors of the leading and trailing piles at $\eta=\theta$=0°, respectively. Obtained from the curve fitting, a_{l0} and a_{t0} are 0.87 and 0.70, respectively. It is noted that the values of a_{l0} and a_{t0} are for two in-line piles with a spacing of 3D. By reference to the maximum pile spacing discussed above, a_{l0} and a_{t0} are both equal to 1 as the pile spacing is larger than 8D. For convenience, both a_{l0} and a_{t0} for pile spacings between 3D and 8D are calculated by linear interpolation.

b_l and b_t are the values of β_l and β_t at $\theta=\theta_c$, respectively. In the range of 90°≥θ≥0°, θ_0 only exists when η≤90°−2φ, so $\theta_c=\theta_0$ and $b_l=b_t$=1; when η>90°−2φ, θ_c=90° and both b_l and b_t are less than 1. Fig. 10 illustrates the values of β at θ=90° obtained from the model tests and the numerical results. As discussed above, β is 1 when η is in the range from 0° to 90°−2φ since θ=90°, which is illustrated by a horizontal line in Fig. 10. As η is also equal to 90°, both piles are placed side by side, and b_l and b_t are equal and newly denoted as b_{90}. Based on the data points in Fig. 10, the relationship between b_l and η in the range from 90°−2φ to 90° was fitted into a straight line. b_{90} for a pile spacing of 3D was taken as 0.90. The fitting curve is plotted in Fig. 10. Because of limited data

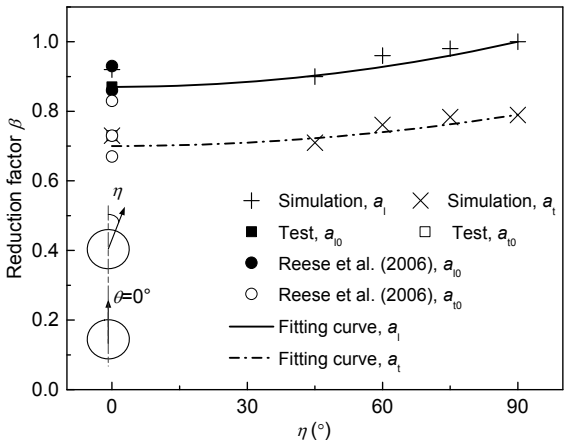

Fig. 9 Relationship between a and η at 3D pile spacing

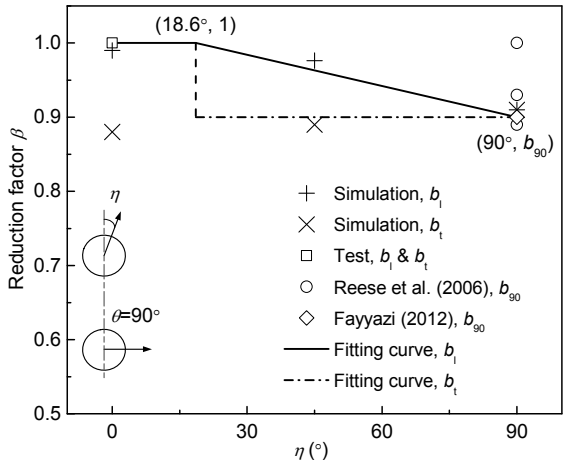

Fig. 10 Relationship between b and η at 3D pile spacing (θ>0°)

points, the variation of b_t with η is not fully figured out. For convenience, b_t in the range from 90°−2φ to 90° is equal to b_{90} (Fig. 10). Similar to a_{l0} and a_{t0}, b_{90} is determined by linear interpolation when the pile spacing is greater than 3D. The maximum spacing proposed by Reese et al. (2006) is 3.75D. In the range $0°>\theta\geq-90°$, since θ_0 always exists as φ is smaller than 45° (Fig. 8), $\theta_c=\theta_0$ and both b_l and b_t are equal to 1. Table 2 summarizes the values or equations of θ_c, b_l, and b_t.

Fig. 6 shows the comparison of the predicted curves by the proposed empirical equations with the present data points. The predicted curves fit the data points fairly well. Particularly, the curves give an indication of the critical angles and the zones with and without interactions.

7.2 Procedure of calculating *p*-multiplier

Given a pile group with n piles subjected to eccentric lateral loading, as the group configuration and the motion directions of all the piles in the group are known, the p-multiplier for each pile can be calculated by Eq. (1). Fig. 11 shows the detailed process.

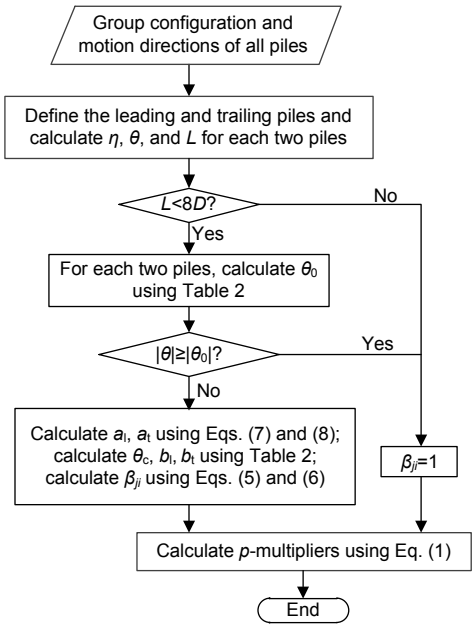

Fig. 11 Flow chart of *p*-multiplier calculation model

In the proposed procedure, only the influence of motion directions on the reduction factors and p-multipliers was considered. In fact, the piles in the group differ not only in motion directions but also in magnitudes. Previous studies on the response of laterally loaded pile groups (McVay et al., 1998; Ashour and Ardalan, 2011) found that p-multipliers decline with the growth of displacement and tend to be constant when displacement is larger than a certain value. A similar feature was also observed from the present centrifuge tests. Therefore, the predicted reduction factors from the proposed empirical equations as well as the calculated p-multipliers usually overestimate the interaction in the piles with small pile displacements. Kong et al. (2015) found that in a pile group subjected to eccentric lateral loading the resistance for the applied lateral load and torque mostly comes from the piles suffering large displacements. Ignoring the effect of pile displacement on reduction factors and p-multipliers, the error in the analysis is limited and on the side of safety.

8 Case study

8.1 2×2 pile group subjected to eccentric lateral loading

Gu (2014) conducted centrifuge model tests on three-diameter spaced 2×2 pile groups subjected to eccentric lateral loading. Model soil was silica sand with relative density of 55%. Model piles were manufactured using aluminum tubes to simulate closed-end pipe piles with an outside diameter of 1.78 m and an embedded pile length of 69.7 m. The flexural stiffness of the piles in the prototype scale was 20.72 GN·m^2. The computer program GROUP 7.0 (Reese et al., 2006) was adopted to simulate the 2×2 pile group under eccentric lateral load with an eccentricity of 7.1D. The computer code, LPILE, was used to back-analyze the soil parameters based on the reported result of a laterally loaded single pile test. The p-y curve model for sand proposed by Reese et al. (1974) was used. The back-calculated internal friction angle and subgrade modulus are 32° and 20000 kN/m^3, respectively. The p-multiplier for each pile in the group was calculated using the proposed approach. The average of the measured torsional resistances of the four piles, which were calculated from the test data, was used in GROUP. The computed

curves of the lateral load-deflection of the pile cap and the pile head shear forces of the individual piles are compared in Fig. 12 with the measured ones. The good agreement between the predicted curves and the experimental data validates the proposed approach for calculating *p*-multiplier.

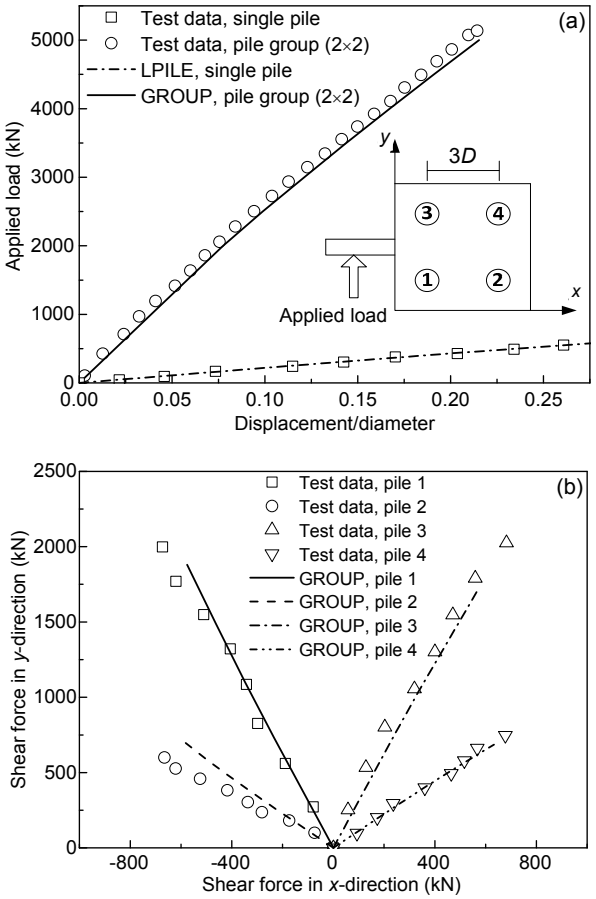

Fig. 12 2×2 pile group subjected to eccentric lateral loading (Gu, 2014)

(a) Applied load-displacement curves of pile group; (b) Pile-head shear forces

8.2 3×3 pile group subjected to eccentric lateral loading

Two large-scale model tests on a three-diameter spaced 3×3 pile group under eccentric lateral loading with different eccentricities (*e*=6*D* and 11*D*) in saturated sandy silt were conducted by Kong et al. (2015). The model piles were fabricated using steel tubes 114 mm in diameter, 4.5 mm in thickness, and 5.95 m in length. The piles were jacked into the soil and fixed by a rigid cap, then horizontally loaded on the pile cap by a hydraulic actuator. GROUP and LPILE were also adopted to simulate the response of the pile groups and back-analyze the soil parameters from a single pile test, respectively. The *p*-*y* curve model proposed by Reese et al. (1974) is also used. The back-calculated internal friction angle and subgrade modulus are 30° and 23 464 kN/m^3, respectively. The measured pile head torsional resistances of all the nine piles were input into GROUP. The comparison between calculated and measured responses of the pile groups is shown in Fig. 13. Reasonably good agreement was achieved for the pile group with lateral loading eccentricity of 6*D*. Agreement was also reasonably favorable at a lateral displacement of up to 0.2*D* for the pile group with a loading eccentricity of 11*D*.

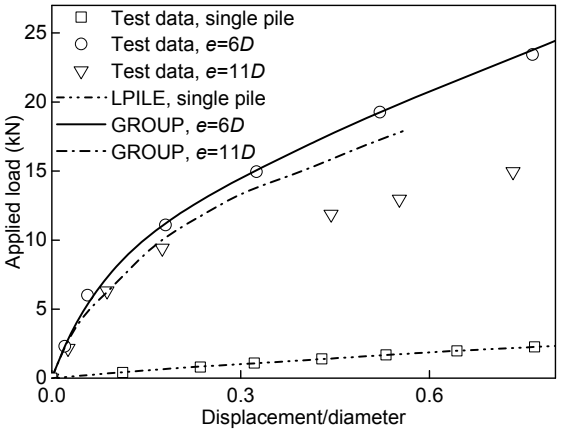

Fig. 13 3×3 pile group subjected to eccentric lateral loading (Kong et al., 2015)

9 Conclusions

Unlike a laterally loaded pile group, piles in a pile group subjected to eccentric lateral loading have different motion directions and magnitudes due to the twist of the pile cap. To study pile-soil-pile interaction due to horizontal motions of two individual piles in a pile group subjected to eccentric lateral loading, concepts of the leading pile and the trailing pile were defined to characterize the relative positions of the two piles. Centrifuge model tests, numerical analysis by ABAQUS, and theoretical analysis were carried out to study interaction between the leading pile and

the trailing pile. The following findings and conclusions are summarized from the present study:

1. Any two piles in a pile group subjected to eccentric lateral loading can be classified as a leading pile and a trailing pile. The angles between the motion directions of the leading and trailing piles and the line through both piles, denoted as η and θ, vary in the ranges 0°–90° and −90°–90°, respectively.

2. The experimental and numerical results show that the reduction factors of the leading and the trailing piles both vary nonlinearly with η and θ. If interaction between two piles exists, the reduction factor of the leading pile is larger than that of the trailing pile.

3. Both the theoretical analysis using a revised wedge failure model and the present tests demonstrate that there exist regions without the interaction between two piles in the η-θ plane. The critical angle θ_0 was introduced to define the boundary with and without interaction for a given η.

In addition, empirical equations of reduction factors for sand and a procedure to calculate *p*-multiplier were proposed in this paper. Centrifuge and 1-*g* model tests on pile groups subjected to eccentric lateral loading were analyzed, and the results showed reasonably good agreement with the measured values.

References

Ashour M, Ardalan H, 2011. Employment of the *p*-multiplier in pile-group analysis. *Journal of Bridge Engineering*, 16(5):612-623. https://doi.org/10.1061/(ASCE)BE.1943-5592.0000196

Bolton MD, 1986. The strength and dilatancy of sands. *Géotechnique*, 36(1):65-78. https://doi.org/10.1680/geot.1986.36.1.65

Brown DA, Morrison C, Reese LC, 1988. Lateral load behavior of pile group in sand. *Journal of Geotechnical Engineering*, 114(11):1261-1276. https://doi.org/10.1061/(asce)0733-9410(1988)114:11(1261)

Cai SW, 2011. Centrifuge Modeling of System Performance of Bridge Foundations in Inland Waterways Subject to Vessel Collision. MS Thesis, The Hong Kong University of Science and Technology, Hong Kong, China.

Chen SL, Kong LG, Zhang LM, 2016. Analysis of pile groups subjected to torsional loading. *Computers and Geotechnics*, 71:115-123. https://doi.org/10.1016/j.compgeo.2015.09.004

Cheng YM, Hu YY, 2005. Active earth pressure on circular shaft lining obtained by simplified slip line solution with general tangential stress coefficient. *Chinese Journal of Geotechnical Engineering*, 27(1):110-115. https://doi.org/10.3321/j.issn:1000-4548.2005.01.019

Craig WH, Sabagh SK, 1994. Stress-level effects in model tests on piles. *Canadian Geotechnical Journal*, 31(1):28-41. https://doi.org/10.1139/t94-004

Fayyazi MS, Taiebat M, Finn WDL, et al., 2012. Evaluation of *p*-multiplier method for performance-based design of pile groups. Proceedings of the 2nd International Conference on Performance-based Design in Earthquake Geotechnical Engineering.

Gu M, 2014. Model Test Study on Behavior of Pile Group Subjected to Lateral Cyclic and Eccentric Loads. PhD Thesis, Zhejiang University, Hangzhou, China (in Chinese).

Hu ZH, McVay M, Bloomquist D, et al., 2006. Influence of torque on lateral capacity of drilled shafts in sands. *Journal of Geotechnical and Geoenvironmental Engineering*, 132(4):456-464. https://doi.org/10.1061/(asce)1090-0241(2006)132:4(456)

Kong LG, Zhang LM, 2007a. Centrifuge modeling of torsionally loaded pile groups. *Journal of Geotechnical and Geoenvironmental Engineering*, 133(11):1374-1384. https://doi.org/10.1061/(asce)1090-0241(2007)133:11(1374)

Kong LG, Zhang LM, 2007b. Rate-controlled lateral-load pile tests using a robotic manipulator in centrifuge. *Geotechnical Testing Journal*, 30(3):192-201. https://doi.org/10.1520/GTJ13138

Kong LG, Zhang LM, 2008. Experimental study of interaction and coupling effects in pile groups subjected to torsion. *Canadian Geotechnical Journal*, 45(7):1006-1017. https://doi.org/10.1139/T08-038

Kong LG, Chen RP, Wang SH, et al., 2015. Response of 3×3 pile groups in silt subjected to eccentric lateral loading. *Journal of Geotechnical and Geoenvironmental Engineering*, 141(7):04015029. https://doi.org/10.1061/(ASCE)GT.1943-5606.0001313

McVay M, Zhang LM, Molnit T, et al., 1998. Centrifuge testing of large laterally loaded pile groups in sands. *Journal of Geotechnical and Geoenvironmental Engineering*, 124(10):1016-1026. https://doi.org/10.1061/(asce)1090-0241(1998)124:10(1016)

Otani J, Pham KD, Sano J, 2006. Investigation of failure patterns in sand due to laterally loaded pile using X-ray CT. *Soils and Foundations*, 46(4):529-535. https://doi.org/10.3208/sandf.46.529

Reese LC, Cox WR, Koop FD, 1974. Analysis of laterally loaded piles in sand. Proceedings of the 6th Annual Offshore Technology Conference, p.473-485. https://doi.org/10.4043/2080-MS

Reese LC, Wang ST, Vasquez L, 2006. Computer Program GROUP 7.0—Technical Manual: Analysis of a Group of Piles Subjected to Axial and Lateral Loading. Ensoft, Inc., Austin, Texas, USA.

Rollins KM, Lane JD, Gerber TM, 2005. Measured and computed lateral response of a pile group in sand. *Journal of Geotechnical and Geoenvironmental Engineering*, 131(1):103-114. https://doi.org/10.1061/(asce)1090-0241(2005)131:1(103)

中文概要

题　目：水平偏心受荷桩基础在砂土中的群桩效应

目　的： p 乘子法在水平受荷群桩非线性静力响应分析中应用广泛，是定量表征水平受荷群桩中群桩效应影响的有效方法。本文基于水平偏心受荷群桩中群桩效应的理论、实验和数值分析成果，提出一套定量表征水平偏心受荷群桩群桩效应的 p 乘子经验算法（为区别于水平受荷群桩 p 乘子，该 p 乘子被命名为广义 p 乘子）。

创新点： 1. 提出表征水平偏心受荷群桩群桩效应的 p 乘子经验算法；2. 分析水平偏心受荷群桩中任意两桩的运动规律，给出两桩运动方向角变化范围；3. 给出两桩间产生桩-土-桩相互作用的临界条件。

方　法： 1. 通过理论分析给出两桩运动方向角变化范围和两桩间产生桩-土-桩相互作用的临界条件；2. 利用离心模型实验和数值模拟获得折减系数随两桩运动方向的变化规律；3. 采用数值拟合方法在相互作用存在的方向角范围内建立折减系数随两桩运动方向与两桩连线夹角之间的定量关系。

结　论： 1. 水平偏心受荷的两根桩，前桩运动方向与两桩连线之间的夹角 η 介于 0°到 90°之间，而后桩夹角 θ 介于−90°到 90°之间；2. η 和 θ 组合存在一个范围，在该范围内两桩存在相互作用，且相互作用对后桩的影响往往大于对前桩的影响；3. 实验案例验证了本文提出的广义 p 乘子经验计算公式的合理性。

关键词： 水平偏心；群桩效应；广义 p 乘子；折减系数；离心实验